Temperature Dependence of Peptide Conformational Equilibria from Simulations at a Single Temperature

Ankita Katiyar and Ward H. Thompson[*]

Department of Chemistry, University of Kansas, Lawrence, KS 66045, USA

E-mail: wthompson@ku.edu

Abstract

Understanding the structure of proteins is key to unraveling their function in biological processes. Thus, significant attention has been paid to the calculation of conformational free energies. In this Paper, we demonstrate a simple extension of fluctuation theory that permits the calculation of the temperature derivative of the conformational free energy, and hence the internal energy and entropy, from single-temperature simulations. The method further enables the decomposition into the contribution of different interactions present in the system to the internal energy surface. We illustrate the method for the canonical test system of alanine dipeptide in aqueous solution, for which we examine the free energy as a function of two dihedral angles. This system, like many, is most effectively treated using accelerated sampling methods and we show how the present approach is compatible with an important class of these, those that introduce a bias potential, by implementing it within metadynamics.

Introduction

Small peptides have been widely used as model systems for describing many biophysical processes including conformational equilibrium, protein folding/unfolding, and protein-ligand binding.[1–5] Alanine polypeptides, in particular, have been frequently used to study con-

formational equilibria in biomolecules because they span the important conformations of proteins.[6–11] In solution, these conformational states are in equilibrium and the probability of finding the biomolecule in a particular state is related to its free energy. Therefore, it is of fundamental importance to accurately compute the conformational free energy profiles. In addition, the energetic and entropic driving forces underlying the free energy are key to a mechanistic understanding of the preferred protein conformations.

The conformational free energy of alanine dipeptide (AD) in vacuum and in solution has been extensively investigated in previous experimental and computational studies. The AD molecule has 22 atoms and is highly flexible because of the "soft" dihedrals. A Ramachandran map permits identification of the different conformations of AD as a function of the two dihedral angles Φ and Ψ. These angles are shown in Fig. 1 along with the pictorial representation of the four most populated conformations in aqueous solution: polyproline II (P_{II}), right-handed α helix (α_P and α_R), β-sheet (C_5), and left-handed α helix (α_L) and the two most populated states in the gas phase, C_7^{ax}, and C_7^{eq}, which are stabilized by an intramolecular hydrogen bond (H-bond).

Experimental studies using IR, NMR, and Raman spectroscopy suggest that the P_{II} conformer is the most stable in water, followed by the C_5 conformer, and then by α_P and α_R.[8–12]
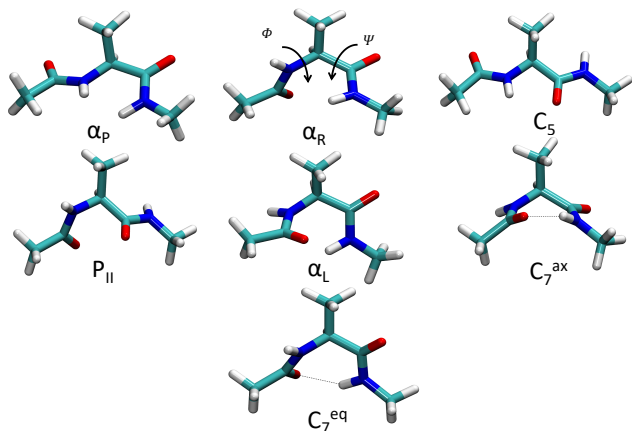
1

Figure 1: Stick models for the most populated conformations of alanine dipeptide in aqueous solution, α_P, α_R, P_{II}, β, α_L, and the gas phase, C_7^{ax}, and C_7^{eq}. The relevant dihedral angles, Φ and Ψ, of the molecule are also shown. Colors: C (cyan), O (red), N (blue), and H (white).

Computational studies have identified the P_{II}, α_P, α_R, and C_5 conformers as lowest in energy.[13–17] Variations in computational methods, AD force-field parameters, water models, and approximations have lead to variations in the energy ordering of these conformers predicted by different simulations. Nevertheless, computational studies provide important insight into the conformational free energy surface, particularly through examination of the energetic and entropic contributions including effect of solvation and the inter- and intra-molecular interactions.

Computational simulations to explore the entire conformational free energy surface are challenging because the conformational transitions occur on a millisecond to second timescale in biomolecules. In a large family of enhanced sampling methods, well-tempered metadynamics (WTmetaD) is widely used to enhance the efficiency of the calculation by facilitating the conformational interconversion using a time-dependent bias potential.[18–20]

Many prior computational studies have focused on the overall effects of solvation on the conformational free energy surface.[21–26] However, very little attention has been given to elucidating the cooperation and competition between the different interactions that determine the free energy in solution, which is a key aim of the present work. Energetic and entropic contributions play an important role in determining the free energy profile of alanine dipeptide as well as different interactions within the system, e.g., solute-solute, solute-solvent, and solvent-solvent. Together these interactions determine the relative stability of different conformers. In a recent study, free energy maps were decomposed into the energetic and entropic components for alanine dipeptide in the gas phase.[27] Another study used 3D-RISM theory to compute the energetic and entropic contribution in the free energy of alanine dipeptide in water. This work showed that the hydration of alanine dipeptide is energetically driven and entropic contributions to the free energy surface are relatively small. However, this method requires simulation at different temperatures to find these contributions.[28]

In this work, we present a simple extension of fluctuation theory to decompose the free energy surface into its enthalpic and entropic component from simulations at a single temperature. Furthermore, we rigorously decompose the internal energy into components associated with different interactions. We consider both broad categories of contributions to the potential energy, i.e., $AD - AD$, $AD - water$, and $water - water$ terms, as well as more specific components of these, e.g., Lennard-Jones and Coulombic interactions. Finally, we show that we can predict conformational equilibria at different temperatures from a single temperature WTmetaD simulation within the van't Hoff approximation.

Theory

Temperature Derivative of the Probability Density

We assume that the molecular conformations of a system can be characterized in terms of a small set of collective variables (CVs), $\mathbf{x}$. We can then obtain the probability density for these variables from molecular dynamics (MD) simu-

lations as

$$P(\mathbf{x}) = \langle \delta[\mathbf{x} - \tilde{\mathbf{x}}(\mathbf{q})] \rangle, \qquad (1)$$

where $\tilde{\mathbf{x}}(\mathbf{q})$ represents the CVs when the system coordinates are given by $\mathbf{q}$ and $\langle...\rangle$ represents a canonical ensemble average. The temperature dependence of this distribution can more clearly be seen by writing the explicit average,

$$
\begin{aligned}
P(\mathbf{x}) &= \frac{h^{-3N} \int d\mathbf{p} \int d\mathbf{q} e^{-\beta H(\mathbf{p},\mathbf{q})} \delta[\mathbf{x} - \tilde{\mathbf{x}}(\mathbf{q})]}{h^{-3N} \int d\mathbf{p} \int d\mathbf{q}\, e^{-\beta H(\mathbf{p},\mathbf{q})}}, \\
&= \frac{1}{Q h^{3N}} \int d\mathbf{p} \int d\mathbf{q} e^{-\beta H(\mathbf{p},\mathbf{q})} \delta[\mathbf{x} - \tilde{\mathbf{x}}(\mathbf{q})]
\end{aligned}
\qquad (2)
$$

where $\beta = 1/k_b T$, H is the Hamiltonian, $\mathbf{p}$ the system momenta, and Q the canonical partition function. Note that the temperature dependence of the distribution occurs only in Q and the Boltzmann weighting in the phase space integral in the numerator. Our group[29,30] and others[31–33] have previously shown how this can be exploited to directly calculate the derivative of such a static average, *e.g.*, the radial distribution function, with respect to temperature (or β).

In the case of alanine dipeptide and other biomolecule systems it is generally necessary to use accelerated sampling methods to determine the free energy surface. Some approaches, such as replica exchange,[34] can give the temperature dependence as a direct result through simultaneous explicit simulation at different T. Here we focus on umbrella sampling-based methods, which introduce a bias potential, $\Delta V(\mathbf{x})$, that is a function of the CVs. In the Results and Discussion we particularly consider the WTmetaD approach where ΔV is history dependent, but the following is applicable to umbrella sampling methods generally. Assuming that the system is in equilibrium with the bias potential, the probability distribution can be written as

$$P(\mathbf{x}) = \frac{\langle e^{\beta \Delta V} \delta[\mathbf{x} - \tilde{\mathbf{x}}(\mathbf{q})] \rangle_{\Delta V}}{\langle e^{\beta \Delta V} \rangle_{\Delta V}}, \qquad (3)$$

where ΔV is the bias potential. The subscript ΔV on the average indicates that the sampling

is carried out under the modified Hamiltonian $H + \Delta V$. We can write the probability distribution more explicitly as

$$P(\mathbf{x}) = \frac{\text{Tr}\left\{e^{-\beta(H+\Delta V)} e^{\beta \Delta V} \delta[\mathbf{x} - \tilde{\mathbf{x}}(\mathbf{q})]\right\}/Q_{\Delta V}}{\text{Tr}\left\{e^{-\beta(H+\Delta V)} e^{\beta \Delta V}\right\}/Q_{\Delta V}}, \qquad (4)$$

where Tr indicates the integration over phase space and $Q_{\Delta V} = \text{Tr}[e^{-\beta(H+\Delta V)}]$ is the partition function for the modified Hamiltonian. We can then examine the (Helmholtz) free energy profile directly from the probability distribution as

$$\Delta A(\mathbf{x}) = -k_b T \ln \frac{P(\mathbf{x})}{P(\mathbf{x}_0)} \qquad (5)$$

where $P(\mathbf{x}_0)$ is the probability density at a reference point of the collective variables. In the next Section, we discuss the thermodynamics and the decomposition of free energy surface into its entropic and energetic contributions.

Temperature Derivative of the Free Energy

The temperature derivative of $\Delta A(\mathbf{x})$ is effectively that of $P(\mathbf{x})$, eq. 3, in which temperature only appears in the Boltzmann weighting, the factor $e^{\beta \Delta V}$ within the average, and the normalizing partition function, $Q_{\Delta V}$. Thus, taking the derivative with respect to β yields

$$
\begin{aligned}
\frac{\partial P(\mathbf{x})}{\partial \beta} &= \frac{1}{\langle e^{\beta \Delta V} \rangle_{\Delta V}} \left[\frac{\partial}{\partial \beta} \langle e^{\beta \Delta V} \delta[\mathbf{x} - \tilde{\mathbf{x}}(\mathbf{q})] \rangle_{\Delta V} \right. \\
&\quad \left. - P(\mathbf{x}) \frac{\partial}{\partial \beta} \langle e^{\beta \Delta V} \rangle_{\Delta V} \right].
\end{aligned}
\qquad (6)
$$

The temperature derivative in the first term of this expression is given by

$$
\begin{aligned}
&\frac{\partial}{\partial \beta} \langle e^{\beta \Delta V} \delta[\mathbf{x} - \tilde{\mathbf{x}}(\mathbf{q})] \rangle_{\Delta V} \\
&= \frac{\partial}{\partial \beta} \left[\frac{1}{Q_{\Delta V}} \text{Tr}\left\{ e^{-\beta(H+\Delta V)} e^{\beta \Delta V} \delta[\mathbf{x} - \tilde{\mathbf{x}}(\mathbf{q})] \right\} \right] \\
&= -\frac{1}{Q_{\Delta V}} \frac{dQ_{\Delta V}}{d\beta} \langle e^{\beta \Delta V} \delta[\mathbf{x} - \tilde{\mathbf{x}}(\mathbf{q})] \rangle_{\Delta V} \\
&\quad - \frac{1}{Q_{\Delta V}} \text{Tr}\left\{ e^{-\beta(H+\Delta V)} e^{\beta \Delta V} H \delta[\mathbf{x} - \tilde{\mathbf{x}}(\mathbf{q})] \right\}.
\end{aligned}
\qquad (7)
$$

3

However, the derivative of the partition function gives the average energy associated with the modified Hamiltonian, $-d \ln Q_{\Delta V}/d\beta = \langle H + \Delta V \rangle$, so that

$$\frac{\partial}{\partial \beta} \langle e^{\beta \Delta V} \delta[\mathbf{x} - \tilde{\mathbf{x}}(\mathbf{q})] \rangle_{\Delta V}$$
$$= -\langle \delta H \, e^{\beta \Delta V} \delta[\mathbf{x} - \tilde{\mathbf{x}}(\mathbf{q})] \rangle_{\Delta V}$$
$$+ \langle \Delta V \rangle_{\Delta V} \langle e^{\beta \Delta V} \delta[\mathbf{x} - \tilde{\mathbf{x}}(\mathbf{q})] \rangle_{\Delta V} \quad (8)$$

where $\delta H = H - \langle H \rangle$ is the fluctuation in the total energy of the system from its average value. Similarly, it is straightforward to show the analogous result,

$$\frac{\partial \langle e^{\beta \Delta V} \rangle_{\Delta V}}{\partial \beta} = -\langle \delta H \, e^{\beta \Delta V} \rangle_{\Delta V}$$
$$+ \langle \Delta V \rangle_{\Delta V} \langle e^{\beta \Delta V} \rangle_{\Delta V} \quad (9)$$

Substituting these results into eq. 6 gives the result for the derivative of $P(\mathbf{x})$ as

$$\frac{\partial P(\mathbf{x})}{\partial \beta} = -\frac{\langle \delta H \, e^{\beta \Delta V} \delta[\mathbf{x} - \tilde{\mathbf{x}}(\mathbf{q})] \rangle_{\Delta V}}{\langle e^{\beta \Delta V} \rangle_{\Delta V}}$$
$$+ \frac{\langle \delta H \, e^{\beta \Delta V} \rangle_{\Delta V}}{\langle e^{\beta \Delta V} \rangle_{\Delta V}} P(\mathbf{x})$$
$$\equiv -P_H(\mathbf{x}) \quad (10)$$

Within a sign, we denote this derivative as $P_H(\mathbf{x})$ and note that it is given by how the occurrence of a particular set of CV values $\mathbf{x}$ is correlated with high ($\delta H > 0$) or low ($\delta H < 0$) energy present in the system relative to the average value. (Note that the derivative does not involve a $\delta \Delta V$ term because its effect in the derivative of the Boltzmann weighting cancels the derivative of $e^{\beta \Delta V}$; in addition, the terms involving $\langle \Delta V \rangle_{\Delta V}$ in eqs. 8 and 9 cancel in eq. 6.)

The free energy contains both energetic and entropic contributions. For the Helmholtz free energy,

$$\Delta A(\mathbf{x}) = \Delta U(\mathbf{x}) - T \Delta S(\mathbf{x}), \quad (11)$$

where $\Delta U(\mathbf{x})$ and $\Delta S(\mathbf{x})$ are the internal energy and entropy, respectively, as a function of the CVs. Taking the derivative of $\Delta A(\mathbf{x})$ in eq. 11 with respect to β and using eqs. 5 and 10,

$$\frac{\partial \Delta A(\mathbf{x})}{\partial \beta} = k_b T \left[\frac{P_H(\mathbf{x})}{P(\mathbf{x})} - \frac{P_H(\mathbf{x}_0)}{P(\mathbf{x}_0)} - \Delta A(\mathbf{x}) \right]. \quad (12)$$

This derivative can be used to evaluate the internal energy and entropy terms. It is straightforward to show that, assuming $\Delta U(\mathbf{x})$ and $\Delta S(\mathbf{x})$ are temperature independent, this yields,[29]

$$\Delta U(\mathbf{x}) = \frac{P_H(\mathbf{x})}{P(\mathbf{x})} - \frac{P_H(\mathbf{x_0})}{P(\mathbf{x_0})}, \quad (13)$$

and

$$\Delta S(\mathbf{x}) = \frac{1}{k_b T^2} \frac{\partial \Delta A(\mathbf{x})}{\partial \beta}. \quad (14)$$

Thus, the energetic and entropic contributions to the free energy can be obtained by the single derivative, $P_H(\mathbf{x})$. A simple method for fitting $\Delta A(\mathbf{x})$, its derivatives, and, hence, $\Delta U(\mathbf{x})$ and $\Delta S(\mathbf{x})$ for peptide conformational equilibria is described in the Appendix.

This approach can also be extended to decompose δH into an additive sum of terms based on different interactions in the system. For example, for alanine dipeptide in dilute aqueous solution, the energy fluctuation can be written as

$$\delta H = \delta KE + \delta V_{AD-AD} + \delta V_{AD-w} + \delta V_{w-w}, \quad (15)$$

where δKE, δV_{AD-AD}, δV_{AD-w}, and δV_{w-w} are the fluctuations in the total system kinetic energy and the $AD - AD$, $AD - water$, and $water - water$ potential energies, respectively. Using this expression for δH in eq. 10 gives the contributions to the temperature derivative of the probability density, which, with eq. 13, gives the components of the internal energy

$$\Delta U(\mathbf{x}) = \Delta U_{KE}(\mathbf{x}) + \Delta U_{AD-AD}(\mathbf{x})$$
$$+ \Delta U_{AD-w}(\mathbf{x}) + \Delta U_{w-w}(\mathbf{x}). \quad (16)$$

Here, for example $\Delta U_{w-w} = P_{w-w}(\mathbf{x})/P(\mathbf{x})$ where $P_{w-w}(\mathbf{x})$ is the same as $P_H(\mathbf{x})$ in eq. 10 with δH replaced by δV_{w-w}. Note that the contribution from the kinetic energy, $\Delta U_{KE}(\mathbf{x})$, is rigorously zero because the CVs depend only on coordinates and not momenta.

Computational Methods

Seven independent well-tempered metadynamics[18,19] (WTmetaD) simulations of alanine dipeptide in water were carried out at 280, 290, 300, 320, 330, 350, and 370 K. The atomistic model of alanine dipeptide was built using the Assisted Model Building with Energy Refinement (AMBER)99 force field.[35] One molecule of alanine dipeptide was solvated in a simulation cell with 372 TIP3P water molecules[36] (1138 total atoms) with cubic periodic boundary conditions. All simulations were performed using GROMACS[37] (v2019.4) patched with PLUMED[38] (v2.6.0).

Before the production simulation, the system was energy minimized for 5,000 steps by steepest descent followed by a 0.5 ns NVT equilibration. The system was then equilibrated in the NpT ensemble for 0.5 ns. Finally, the production MD simulations were initiated from the end of this equilibration (resulting in a volume of 500 Å^3, which is close to the average over the NpT simulation) in an NVT ensemble for 100 ns for each temperature except 300 K. For better sampling in computing the derivatives with respect to temperature, we propagated five 100 ns simulations at 300 K; the convergence properties are presented in the Supporting Information.

All simulations used a 1 fs timestep and temperature was controlled by coupling to a Nosé-Hoover thermostat.[39,40] with a coupling constant (tau-t) of 1 ps. The initial velocities were generated randomly from a Boltzmann distribution at the desired temperature. The short-range non-bonded interactions were truncated using a distance cutoff of 10 Å. Long-range interactions were incorporated by the particle mesh Ewald (PME) method[41] using a grid spacing of 1.1 Å.

Two dihedral angles, Φ and Ψ shown in Fig. 1, were selected as the collective variables (CVs) for the WTmetaD simulations. The WTmetaD simulations were carried out by depositing Gaussians in the defined CV space every 2,000 steps. The initial height of the Gaussian was set to 1.2 kJ/mol and the width was set to 0.35 rad for both Φ and Ψ. The bias factor for WTmetaD was set to 6.0.

Errors are reported as 95% confidence intervals according to the Student's t-distribution[42] obtained using block averaging based on five blocks obtained by dividing the 100 ns trajectory or, at 300 K, using the five 100 ns trajectories as blocks.

Results and Discussion

Conformational Free Energy Surface

We have used WTmetaD simulations to obtain the conformational free energy surface at 300 K of alanine dipeptide in water as a function of the dihedral angles Φ and Ψ, which is shown in Fig. 2. This two-dimensional Ramachandran plot reveals several local minima in the free energy labeled as α_P, α_R, P_{II}, β, and α_L following the notation of Ref. 17.

The free energy surface shows that the right-handed α-helix conformations, α_P and α_R, are more stable than the β-sheet conformations, C_5 and P_{II}. This is consistent with previous theoretical studies using AMBER99 force field.[17] The least stable conformation is found to be α_L because of unfavorable chain-chain interactions (see Fig. 1).

The Φ and Ψ coordinates for each local minimum structure along with experimental values from the literature[43] are given in Table 1. The dihedral angles are in good agreement with the experiments for the C_5 and P_{II} conformers, but the Ψ value differs for α_R. However, the present result agrees with the previous theoretical studies,[17,28] indicating that this discrepancy is attributable to the force field. Quantitatively, the lowest free energy corresponds to the α_P conformer with the free energy of the α_R, P_{II}, C_5, and α_L structures 1.2, 8.1, 5.1, and 12.3 kJ/mol higher in energy, respectively; see Table 2. The positions of these low energy conformations are consistent with the previous experimental studies using Raman optical activity,[44] NMR,[45] and 2D-IR spectroscopy.[46]

One-dimensional free energy profiles with respect to Φ and Ψ are also presented in Fig. 2
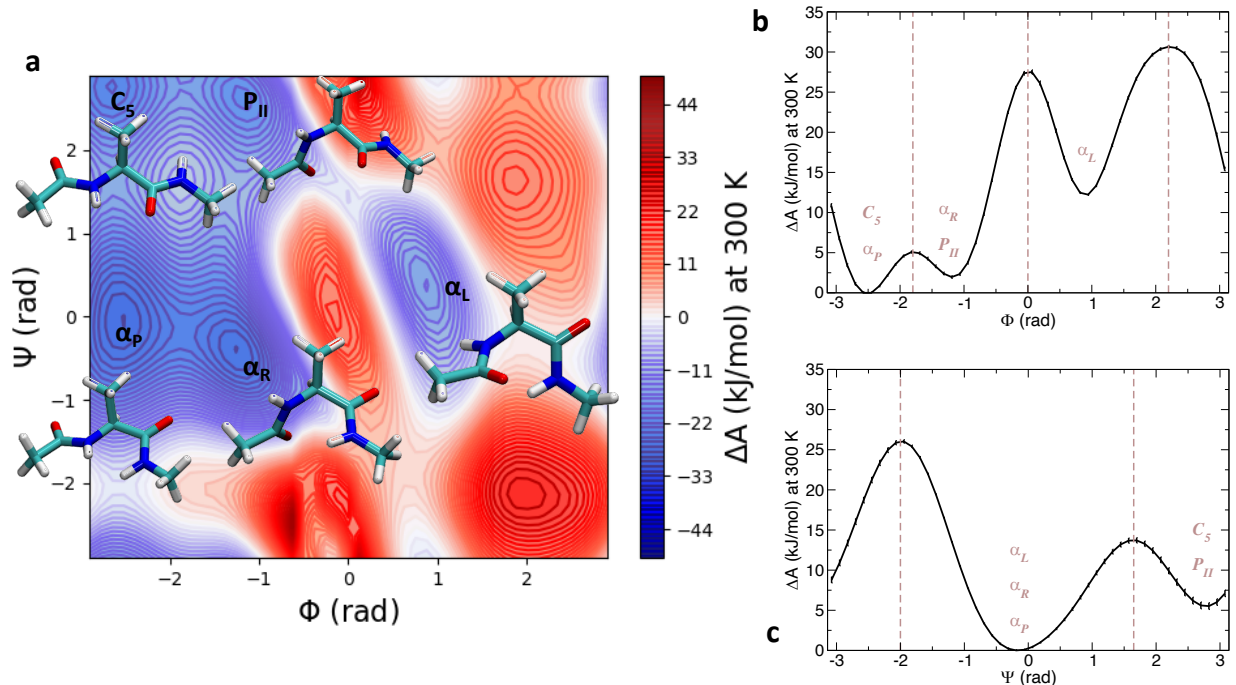
Figure 2: Free energy of alanine dipeptide in water at 300 K as a function of the dihedral angles defined in Fig. 1 shown as the (a) two-dimensional surface and one-dimensional (b) Φ and (c) Ψ profiles. In the contour plot, contour lines are drawn every 1 kJ/mol and five major conformers are labeled with the structures shown.

and show three and two minima, respectively. Comparison with the free energy surface in Fig. 2a shows that most of these minima correspond to more than one conformer. Clearly, the existence of several local minima along Φ suggests that sampling of Φ influences the outcome of the one-dimensional free energy in Ψ and vice versa. We also note that free energy as a function of Ψ is lower for the α-helix conformations (α_P, α_R, and α_L) than the β-sheet conformers. On the other hand, as a function of Φ, the β sheet conformations, C_5 and P_{II} have lower free energy along with the right-handed α helix conformations, α_P and α_R; the left-handed α helix conformation, α_L, has significantly higher free energy.

Conformational Internal Energy and Entropy

We next examine the energetic and entropic contribution to the conformational free energy surface from single temperature simulations, obtained from eqs. 13 and 14 as described in

Table 1: The dihedral angles (in radians) of the stable conformations of AD in aqueous solution. Experimental results are from a previous CD and NMR study.[43]

Configuration	WTMetaD (Φ,Ψ)	Experiment (Φ,Ψ)
C_5	(-2.6, 2.6)	(-2.6, 2.6)
P_{II}	(-1.4, 2.6)	(-1.4, 2.6)
α_R	(-1.4, -0.4)	(-1.4, -0.9)
α_P	(-2.6, -0.1)	–
α_L	(0.9, 0.4)	–

Theory. The two-dimensional contour plots of the internal energy, ΔU, and entropy, $-T\Delta S$, contributions at 300 K are shown as a function of the Φ and Ψ dihedral angles in Fig. 3. The internal energy surface, Fig. 3a, is qualitatively and even quantitatively similar to the free energy surface, Fig. 2. In contrast, the entropic contributions, Fig. 3b, are comparatively small and have generally modest effects on the relative stability of the different conformers. The

Table 2: Thermodynamic decomposition of conformational free energies of four stable conformations relative to the α_P conformation in kJ/mol. Values in parentheses represent uncertainties in the trailing digit(s).

Configuration	ΔA	ΔU	$-T\Delta S$
C_5	5.1(4)	5.8(1.3)	−0.7(1.5)
P_{II}	8.1(3)	7.5(1.8)	0.6(1.7)
α_R	1.2(2)	1.6(5)	−0.4(4)
α_P	0	0	0
α_L	12.3(2)	12.9(9)	−0.6(1.1)

relative internal energy and entropy contributions for the different conformations are tabulated in Table 2. These data show that the internal and free energy display the same ordering for the five conformations that correspond to free energy minima. The entropy stabilizes the C_5, α_L, and α_R conformers and destabilizes the P_{II} structure.

For comparison, we have also calculated the internal energy and entropy by a van't Hoff analysis. Specifically, as described in Computational Methods we carried out seven independent WTmetaD simulations at temperatures from 280 to 370 K to calculate the free energy ΔA from eq. 5 as a function of T. Then a linear fit of $\Delta A(T)$ at each set of Φ and Ψ coordinates yields the internal energy, ΔU, and entropy, $-\Delta S$, as the intercept and slope, respectively. These van't Hoff results are compared to the direct calculations (which represent the analytical, rather than numerical, temperature derivative of the free energy) as one-dimensional profiles in Φ and Ψ in Fig. 3c,d. The two calculation methods are in excellent agreement. This demonstrates the equivalence of the present approach involving simulations at a single T with more standard van't Hoff methods based on simulations at different temperatures. As is discussed in detail below, however, the current method enables the decomposition of the internal energy into contributions from the different interactions at play in the system, while the latter approach does not.

While the directly calculated and van't Hoff internal energies and entropies are the same within errors at nearly all values of the dihedral coordinates, some minor deviations are observed for $-0.5\,\text{rad} \leq \Psi \leq 0.8\,\text{rad}$. It is unclear if these are associated with incomplete convergence of the fluctuation theory calculations (though the small uncertainties suggest not) or some temperature dependence of the $\Delta U(\Psi)$ over the range used in the van't Hoff analysis. The convergence of the directly calculated one-dimensional profiles with the simulation time at 300 K is shown in Fig. S3 of the Supporting Information. These results show that quite accurate internal energy and entropy profiles can be obtained from just two or three (100 ns) trajectories (the latter being the minimal number required for a van't Hoff analysis). The ΔU and $-T\Delta S$ obtained from four such trajectories are nearly identical to the results from five trajectories shown in Fig. 3c,d.

Decomposition of the Internal Energy

We now consider the driving forces for the conformational preferences of alanine dipeptide in aqueous solution. We first investigate the solvation effects. It is known that in the gas phase alanine dipeptide has three stable structures, C_5, C_7^{eq}, and C_7^{ax} with locations in the (Φ, Ψ) coordinates at (-2.7, 2.7), (-0.9, 0.6), and (0.9, -0.6).[16,27,28] In particular, the conformational free energy surface is dominated by the C_7^{eq} and C_7^{ax} minima due to the internal H-bonding present in these structures shown in Fig. 1. The C_5 conformer is entropically favored because it allows more conformational flexibility than the folded C_7 conformations. However, as we have discussed above, in aqueous solution using the TIP3P water model the C_7^{eq} conformer is no longer a local minimum, but is instead replaced by the α_R and P_{II} structures. Similarly, the C_7^{ax} conformer that appears in the gas phase is supplanted by the α_L structure.

To investigate these shifts in the free energy minima from the gas phase to solution we consider the decomposition of the internal energy into peptide-peptide ($AD-AD$), peptide-water ($AD-w$), and water-water ($w-w$) interactions as given in eq. 16. The results of these
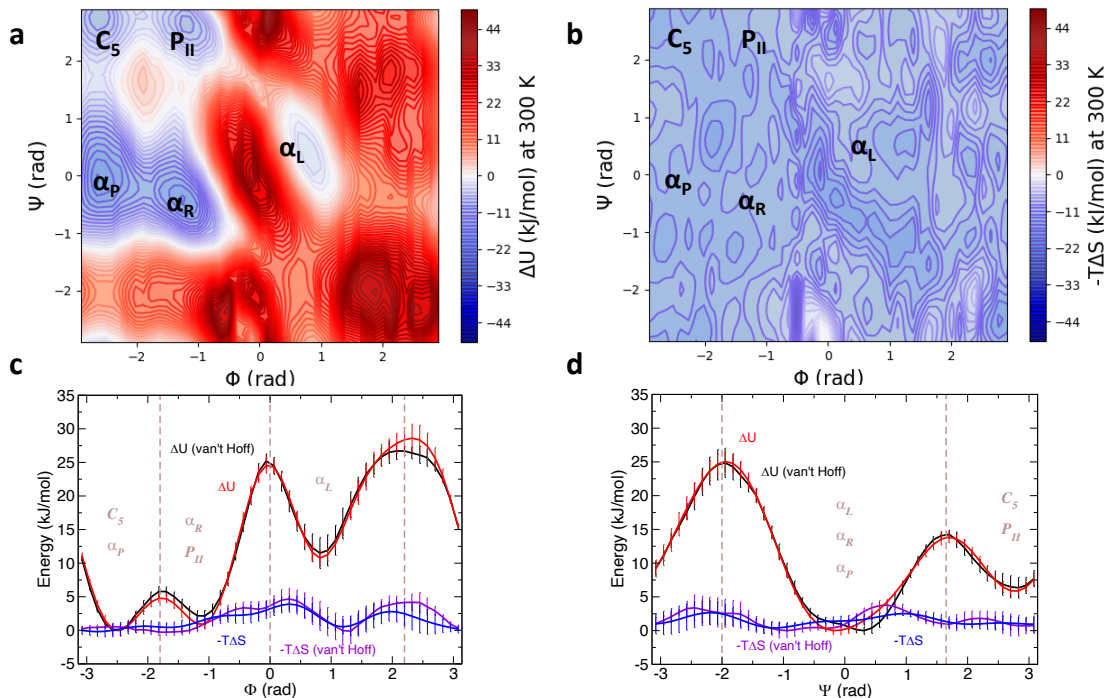
Figure 3: Contour plots of the (a) internal energy, $\Delta U(\Psi, \Phi)$, and (b) entropic contribution, $-T\Delta S(\Psi, \Phi)$ of alanine dipeptide in water at 300 K obtained by the fluctuation method. Contour lines are drawn every 1 kJ/mol. Also shown are one-dimensional plots of the ΔU (red lines) and $-T\Delta S$ (blue lines) as a function of (c) Φ and (d) Ψ; results for ΔU (black lines) and $-T\Delta S$ (violet lines) from a van't Hoff analysis are also shown for comparison.

calculations are shown in Fig. 4 and the data is summarized in Table 3, using the α_P conformer as the reference state. One-dimensional plots of the internal energy components as a function of each of the dihedral angles Φ and Ψ are presented in Fig. 4d,e. These provide a clear comparison of the effect of different interactions on the total internal energy. In particular, they show that the largest contribution to the internal energy comes from the peptide-peptide $(AD - AD)$ potential with significant contributions from the peptide-water $(AD - w)$ interactions that change the relative stability of some of the conformations. We can also see that, although they are small, the water-water contributions are not negligible and largely act in opposition to the $AD - w$ component.

The internal energy due to the peptide-peptide interactions, ΔU_{AD-AD}, is presented in Fig. 4a and exhibits three minima at $(\Phi, \Psi) =$ (-2.7, 2.7), (-0.9, 0.6), and (0.9, -0.6). These are the same conformers that have been identified in the gas-phase alanine dipeptide structure.

Table 3: Thermodynamic decomposition of internal energies of four stable conformations relative to the α_P conformation in kJ/mol. Values in parentheses represent uncertainties in the trailing digit(s).

Configuration	ΔU_{AD-AD}	ΔU_{AD-w}	ΔU_{w-w}
C_5	$-2.9(2)$	$18.5(4)$	$-9.8(1.0)$
P_{II}	$6.3(1)$	$6.4(2)$	$-5.3(1.7)$
α_R	$-4.1(1)$	$11.8(3)$	$-6.1(6)$
α_P	0	0	0
α_L	$10.0(1)$	$5.8(3)$	$-2.9(1.0)$

ture.[16,27,28] The minimum at (-2.7, 2.7) corresponds to the C_5 conformer, which is the third most stable configuration in aqueous solution as shown in Fig. 2. Two new conformations that appear due to intra-peptide interactions are C_7^{eq} and C_7^{ax} at (-0.9, 0.3), and (0.9, -0.6), respectively. We quantitatively compare the contribution of the peptide-peptide interactions to the relative internal energies, ΔU_{AD-AD}, of
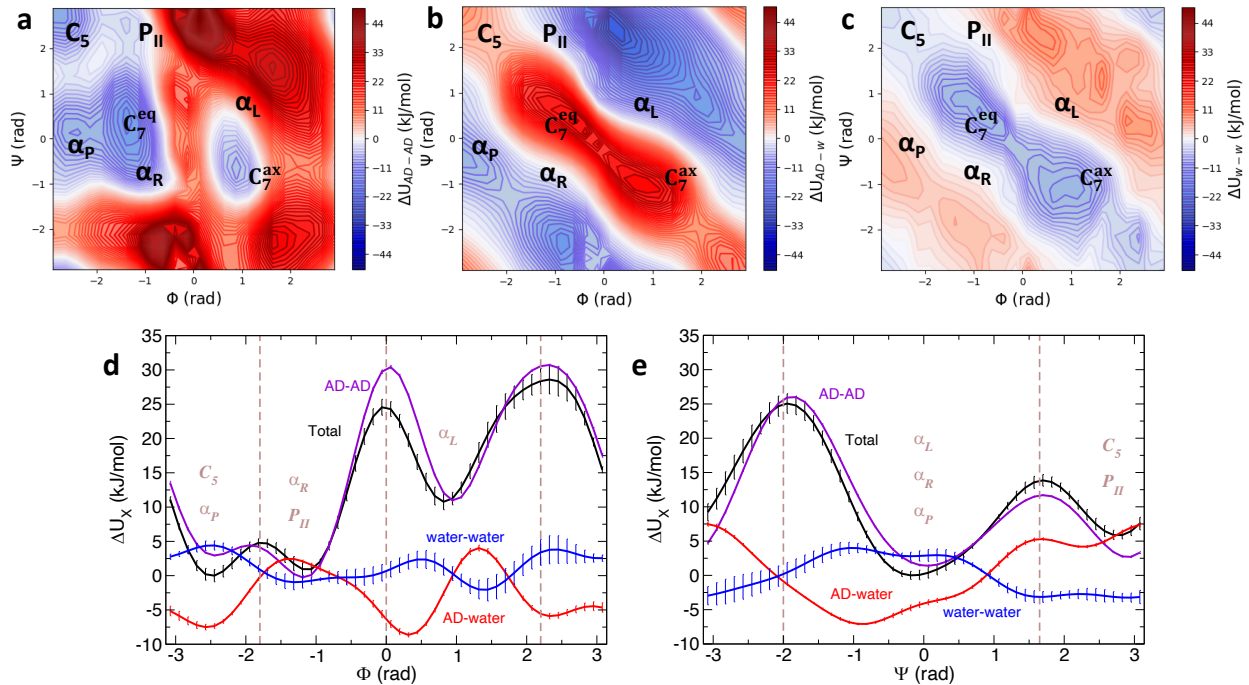
Figure 4: Contribution to the total internal energy at 300 K from (a) AD-AD, (b) AD-water, and (c) water-water interactions shown as two-dimensional contour plots. Contour lines are drawn every 1 kJ/mol. One dimensional internal energy contributions are shown as a function of (d) Φ and (e) Ψ.

the five major states in aqueous solution in Table 3. The data indicate that while the α_P conformer is most stable in aqueous solution, the intrapeptide interactions most strongly favor the α_R structure, which resembles the C_7^{eq} state found in the gas phase due to intramolecular hydrogen bonding. The C_5 conformer is the next most stable based only on the peptide-peptide interactions followed by α_P and the P_{II} and α_L (C_7^{ax}) are significantly less favorable. Note that α_L (C_7^{ax}) has intra-peptide hydrogen bonding, but is least stable due to unfavorable inter-chain interactions.

The change in conformational energetics when moving from the gas-phase to solution is dominated by the peptide-solvent interactions that are encompassed in ΔU_{AD-w}. These alanine dipeptide-water interactions disrupt the intramolecular H-bonding of the folded conformers that are a key piece of the stability in the gas phase in favor of water-peptide H-bonds. The result is a significant reordering of the relative energetics of the dipeptide structures. In particular, the two structures that are

most favored by the intrapeptide interactions, α_R and C_5, are disfavored by approximately 12 and 19 kJ/mol relative to the α_P conformer, respectively, by the direct interactions of the water and peptide. The α_R geometry forms two pockets where water molecules can sit and H-bond with CO–NH units. But, in this case the CO–NH units are arranged at angles that make it harder to form water bridges. In the C_5 case, even though the CO–NH units are nearly coplanar the spatial arrangement also disrupts H-bonded water bridges.

It is important to note, however, that these peptide-water contributions are partially cancelled by the corresponding changes in the water-water component. That is, the ΔU_{w-w} term favors the conformers in exactly the opposite order of the ΔU_{AD-w} energetics. Thus, for both the α_R and C_5 conformers, half of the increase in internal energy (relative to that of the α_P structure) is cancelled by a decrease in the corresponding water-water energy. This still leads to a significant, but quantitatively smaller, destabilization of these structures in

9

aqueous solution.

The energetics of the P_{II} and α_L structures are more modestly affected by the presence of the water. They are destabilized by the peptide-water interactions, but this effect is largely cancelled by the concomitant water-water contribution so that the net increase in internal energy relative to α_P is by approximately 1.1 and 2.9 kcal/mol for P_{II} and α_L, respectively.

These results demonstrate that contributions to the internal energy from all three of these interactions, available within the present fluctuation theory approach, are required to explain the free energy surface of alanine dipeptide in water. We find that α_R is favored by both the $AD - AD$ and $w - w$ and destabilized by the $AD - w$ interactions, making it the second most stable conformation behind α_P. Peptide-peptide and water-water interactions also favor the C_5 conformation which is, however, more strongly disfavored by the interaction of the peptide with the surrounding water molecules. The next most stable conformation, P_{II}, is stabilized by $w - w$ interactions but destabilized by the intrapeptide and $AD - w$ contributions. The least stable α_L configuration has the highest ΔU_{AD-AD} and its internal energy is also modestly increased by the presence of the solvent. This demonstrates that the internal energy ranking of the four main conformations is a consequence of competing and cooperative effects of all three of these interactions.

The present method allows us to further explore the interactions that are responsible for conformational preferences by further decomposition of the internal energy into the individual interaction terms. In the context of the peptide-peptide interactions, there are four different contributions such that

$$
\begin{aligned}
\Delta U_{AD-AD} &= \Delta U_{AD-AD,dih} \\
&+ \Delta U_{AD-AD,ang} + \Delta U_{AD-AD,Coul} \\
&+ \Delta U_{AD-AD,LJ} \quad (17)
\end{aligned}
$$

where dih, ang, $Coul$, and LJ subscripts indicate contributions associated with the $AD - AD$ dihedral angle, bending angle, Coulombic, and Lennard-Jones potential terms, respec-

tively. These components of the internal energy are shown as contour plots in Φ and Ψ in Fig. 5a-d.

It is clear from these data that ΔU_{AD-AD} in Fig. 4a results from considerable cooperation and cancellation between the different intrapeptide interactions. The dominant contributions to ΔU_{AD-AD} come from the dihedral angle and Coulombic potentials (note the different scales on the plots in Fig. 5a-d). The former favors the α-helix structures while the latter has low internal energy contributions only for the C_7^{eq} and C_7^{ax} configurations that are stabilized by an intramolecular H-bond (see Fig. 1). The angle bending contribution, $\Delta U_{AD-AD,ang}$, is negative and modest for nearly all configurations except around $(\Phi, \Psi) \simeq (0,0)$ where it is strongly repulsive. The same region is disfavored by the Lennard-Jones interactions which are lowest for the C_5, P_{II}, and α_R conformers, though the magnitude of the contributions to the internal energy are comparatively small.

It is interesting to note that many of the detailed features of the individual components in eq. 17 are obscured in the one-dimensional internal energy profiles shown in Fig. 5e,f. For example, $\Delta U_{AD-AD,Coul}$ appears small in both one-dimensional curves, but upon examination of Fig. 5c this is clearly a result of cancellation when averaging over Φ (Ψ) for a given value of Ψ (Φ). The same is true for the other potential terms as well, though the contour plots and one-dimensional profiles do both reflect the more modest quantitative contributions of the angle bending and Lennard-Jones interactions to ΔU_{AD-AD}. Overall, the one-dimensional internal energies in Fig. 5e,f indicate that the dihedral potential is, by far, the largest contribution and closely resembles the total ΔU_{AD-AD} as a function of Ψ and is the most significant component of ΔU as a function of Φ.

While $\Delta U_{AD-AD,dih}$ is the largest component of the intrapeptide internal energy as a function of Φ, Fig. 5e, the bending angle and Coulombic potential terms also have major contributions. The bending potential favors the α_L conformers and disfavors the α_R and P_{II} structures while the intrapeptide electrostatics preferentially stabilize the α_L, α_R, and P_{II} structures.
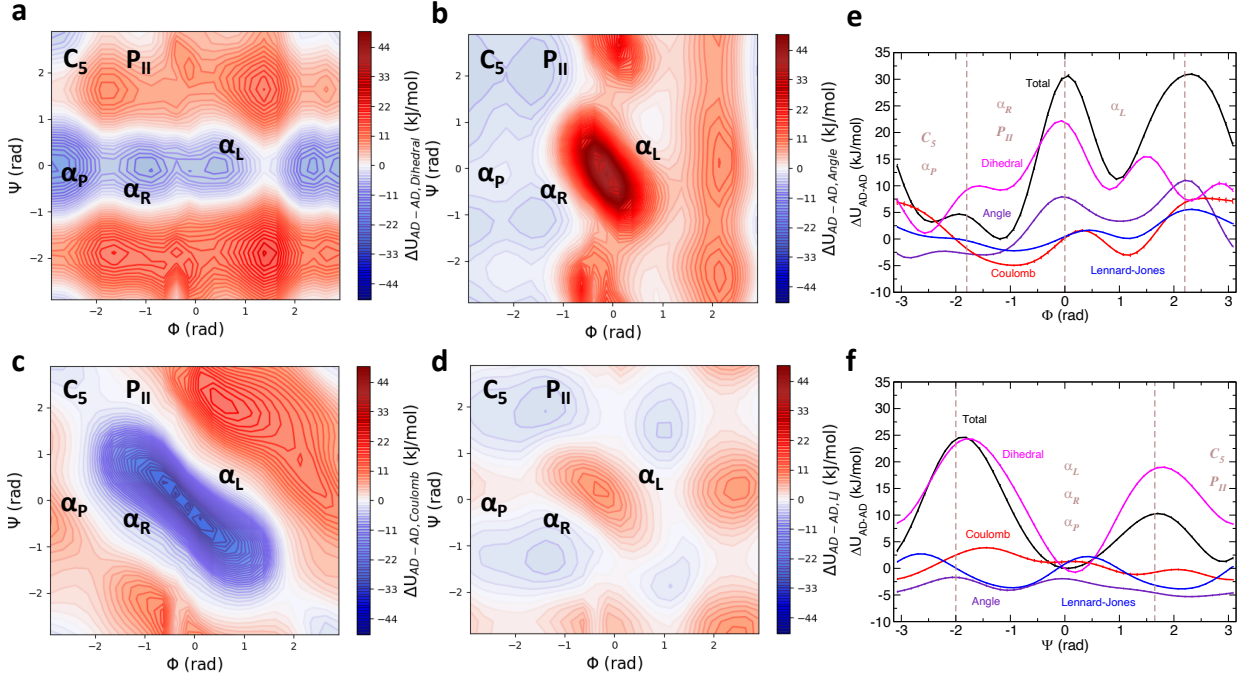
Figure 5: Contributions to the internal energy from the $AD - AD$ (a) dihedral, (b) bending angle, (c) Coulombic, and (d) Lennard-Jones potential energy terms, eq. 17. Contour lines are drawn every 1 kJ/mol. These contributions are also compared to the total ΔU_{AD-AD} as a function of (e) Φ and (f) Ψ.

In the one-dimensional internal energy versus Ψ, Fig. 5f, the dihedral potential strongly favors the α-helix conformations ($\Psi \sim 0.3$ rad) over β-sheet structures ($\Psi \sim 2.6$ rad), while the other three interactions lower the relative free energy of the β-sheet conformations, though not enough to make them the global minimum. Comparing to Fig. 5a-d, however, it is apparent that the actual picture of how the different interactions determine the total ΔU_{AD-AD} is more complex than captured in these one-dimensional profiles.

The relative internal energy due to peptide-water interactions can also be split into two non-bonded interactions,

$$\Delta U_{AD-w} = \Delta U_{AD-w,Coul} + \Delta U_{AD-w,LJ}. \quad (18)$$

These contributions to the internal energy are shown in Fig. 6 as contour plots in Φ and Ψ. The results show clearly that the relative internal energy due to peptide-water interactions is driven almost entirely by electrostatic interactions. The Lennard-Jones contributions are quite modest (note the scale in Fig. 6b) and

only act to slightly destabilize the α-helix and P_{II} conformers.

Interestingly, a comparison of the $AD - AD$ and $AD - w$ Coulombic contributions to the internal energy, shown in Figs. 5c and 6a, respectively, are nearly mirror images. Namely, the intrapeptide electrostatics favor the intramolecularly H-bonded C_7^{eq} and C_7^{ax} configurations, while the same configurations are strongly disfavored by the peptide-water interactions. The latter presumably drive the system toward water-peptide H-bonds instead. Cancellation between $\Delta U_{AD-AD,LJ}$ and $\Delta U_{AD-w,LJ}$ can also be observed in Figs. 5d and 6b, but it is both less qualitatively consistent and quantitatively dramatic. Namely, the Lennard-Jones contributions are significantly smaller than the Coulombic ones and, perhaps because they are not the dominant interactions, need not oppose one another. Instead, a more consistent mirroring is observed between the $AD - w$ Coulombic and Lennard-Jones contributions (Fig. 6). It will be interesting to see how these competitions play out in larger, helix-forming peptides.
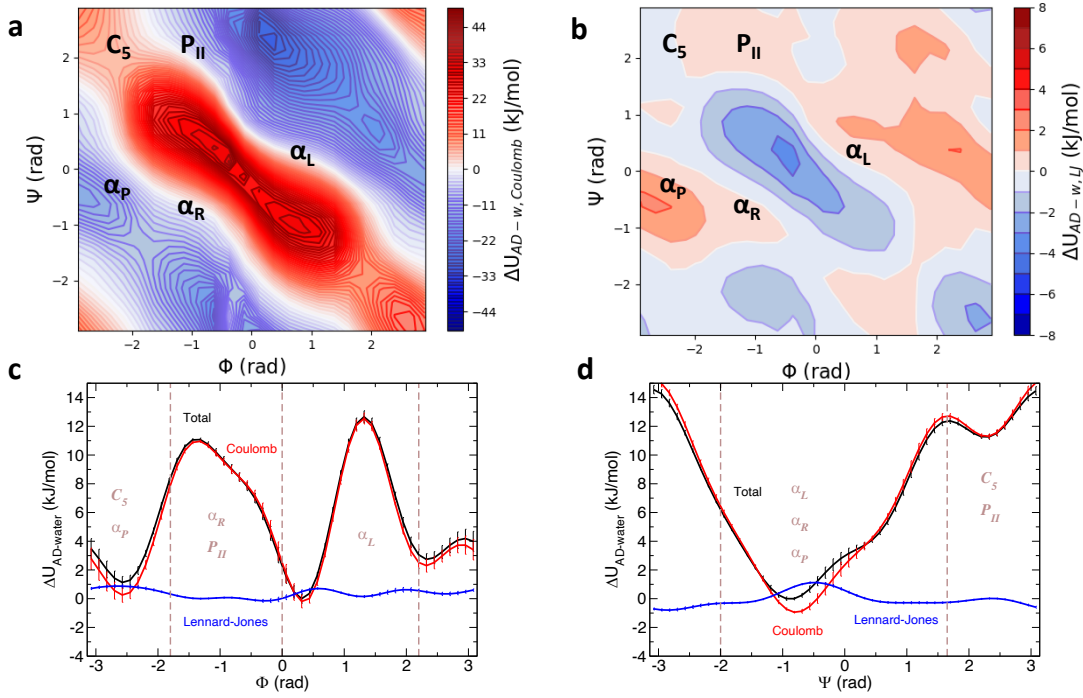
11

Figure 6: Contributions to the internal energy from the $AD-w$ (a) Coulombic and (b) Lennard-Jones potential energy terms, eq. 18. Note that the energy scale for (b) is different from (a). Contour lines are drawn every 1 kJ/mol in both. These contributions are compared to the total ΔU_{AD-w} as a function of (c) Φ and (d) Ψ.

Prediction of Conformational Equilibria at Different Temperatures

Finally, we examine the equilibrium constants between conformers as a function of temperature and use the present approach to predict it from simulations at room temperature alone. The population of a conformer defined by the collective variables $\mathbf{x}$ at a temperature T_2 can be obtained from the corresponding population at T_1 as

$$\begin{aligned} \log P(\mathbf{x}, T_2) &= \log P(\mathbf{x}, T_1) \\ &+ \left(\frac{1}{T_1} - \frac{1}{T_2}\right) \frac{\Delta U(\mathbf{x})}{k_b}, \end{aligned} \quad (19)$$

where ΔU is the internal energy given by eq. 13. This expression makes the van't Hoff assumption that the energetic and entropic contributions are temperature independent.

We have used eq. 19 to calculate the ratio of the α_L, C_5, P_{II}, and α_R populations to that of the α_P conformer as a function of temperature. These are presented in Fig. 7 where they are compared to the results obtained directly from

the individual simulations at six other temperatures. We find that our values obtained from single temperature simulations are in excellent agreement with the calculations at the different temperatures. Because the α_P conformer has the lowest internal energy, as the temperature increases, the relative population of the other three higher energy structures increases. In each case, the slope is given by the relative internal energy and thus, it is largest in the case of the least energetically stable conformer, α_L, for which $\Delta U = 12.9$ kJ/mol relative to α_P and smallest for the most energetically similar, α_R, where $\Delta U = 1.6$ kJ/mol; see Table 2.

These results show that the internal energies are sufficiently accurate to predict the relative conformer populations over a wide range of temperatures (at least $280-370$ K) from the room temperature simulations. Moreover, the decompositions of the internal energy contributions means that we can simultaneously gain mechanistic insight into the origin of the temperature dependence in terms of the different interactions present.
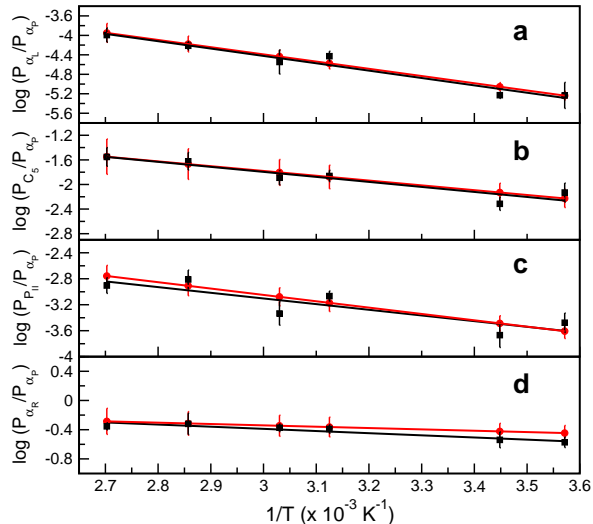
Figure 7: Population ratios expressed as $\log(P_X/P_{\alpha_P})$ for X taken as the (a) α_L, (b) C_5, (c) P_{II}, and (d) α_R conformer as a function of $1/T$. Results are shown for independent simulations at different temperatures (black squares) and predictions from the simulations at 300 K using eq. 19 (red circles). Linear fits are shown as solid lines.

Conclusion

In this work, we have presented a simple fluctuation theory method to explore the conformational free energy surface of alanine dipeptide in water. This method allows us to get deeper insights into the thermodynamic decomposition of important biological systems. We used this method to understand the conformational free energy surface of a prototypical system, alanine dipeptide in water. We decomposed the conformational free energy profile into energetics and entropic contributions from a single temperature simulation at 300 K. We found the internal energy and entropy results from this approach are in excellent agreement with van't Hoff calculations obtained from simulations at different temperatures.

In addition, we decomposed the internal energy into contributions from peptide-peptide, peptide-water, and water-water interactions to understand the cooperative and competing effects of solvation. We also showed that the internal energy can be further subdivided into components associated with individual interaction terms in the system, applying it to gain insight into the origins of the peptide-peptide and peptide-water internal energies. We note that this important mechanistic information cannot be obtained from a traditional van't Hoff approach based on simulations at different temperatures.

Thus, we have presented a simple but powerful method for obtaining detailed information about the driving forces that determine the conformational free energy landscape. It additionally removes the necessity of running simulations at multiple temperatures that is required to obtain even the total energetic and entropic effects. This also means that it can be used in situations where changing the temperature can be problematic, *e.g.*, near a phase or folding transition. It should thus be a useful method to study the effect of intrapeptide interactions and solvation on conformational free energies in longer peptides and more complex biomolecular systems.

Appendix

Here we describe a simple method for fitting the free energy and its derivatives from which the internal energy and entropy can be obtained. The approach described in the Theory section can be applied directly to determine the derivative of the free energy with respect to β within each histogram bin in the CVs. However, we have found that the smoothness and convergence of the derivative, and hence $\Delta U(\mathbf{x})$ and $\Delta S(\mathbf{x})$, are improved by fitting the free energy to an accurate functional form. For the free energy as a function of the Ψ dihedral angle alone, the form

$$\Delta A(\Psi) = A_0 + \sum_{n=1}^{4} A_n \left[\cos(n\Psi - d_n) + 1\right] \quad (20)$$

accurately describes the behavior for alanine dipeptide for the free energy averaged over all

Φ coordinate values. It also represents the two-dimensional free energy, $\Delta A(\Phi, \Psi)$, in which case the amplitudes, A_n, and phase shifts, d_n, are determined separately for, and thus depend on, each value of Φ.

Considering the parameters A_n and d_n in eq. 20 to be temperature dependent, it is straightforward to show that,

$$
\begin{aligned}
\frac{\partial \Delta A(\Psi)}{\partial \beta} &= \frac{\partial A_0}{\partial \beta} \\
&+ \sum_{n=1}^{4} \left\{ \frac{\partial A_n}{\partial \beta} \left[\cos(n\Psi - d_n) + 1 \right] \right. \\
&+ \left. \frac{\partial d_n}{\partial \beta} \left[\sin(n\Psi - d_n) + 1 \right] \right\}. \quad (21)
\end{aligned}
$$

Rearranging eq. 12 and using eq. 13, the internal energy as a function of Ψ can be written as

$$
\Delta U(\Psi) = \beta \frac{\partial \Delta A(\Psi)}{\partial \beta} + \Delta A(\Psi). \quad (22)
$$

Substituting eqs. 20 and 21 into this expression yields

$$
\begin{aligned}
\Delta U(\Psi) &= \left[A_0 + \beta \frac{\partial A_0}{\partial \beta} \right] \quad (23) \\
&+ \sum_{n=1}^{4} \left\{ \left[A_n + \beta \frac{\partial A_n}{\partial \beta} \right] \right. \\
&\times \left[\cos(n\Psi - d_n) + 1 \right] \\
&+ \left. \beta \frac{\partial d_n}{\partial \beta} \left[\sin(n\Psi - d_n) + 1 \right] \right\}.
\end{aligned}
$$

In practice, we first fit $\Delta A(\Psi)$ obtained from $P(\Psi)$ to eq. 20 to determine the A_n and d_n. Then, we compute $\Delta U(\Psi)$ from $P(\Psi)$ and $P_H(\Psi)$ from eq. 13 and fit the result to eq. 23 in which the A_n and d_n are fixed to the values obtained by fitting $\Delta A(\Psi)$ and only $\partial A_n/\partial \beta$ and $\partial d_n/\partial \beta$ are allowed to vary. The entropic contribution is then calculated as $-T\Delta S(\Psi) = \Delta A(\Psi) - \Delta U(\Psi)$. For the two-dimensional surface, $\Delta U(\Phi, \Psi)$, the fitting process is carried out for the Ψ dependence for each fixed value of Φ.

The same approach is used to fit $\Delta A(\Phi)$, but the more complicated form of the free energy compared to $\Delta A(\Psi)$ requires five cosine terms instead of four.

Supporting Information

Plots of results obtained without the fitting described in the Appendix and of the convergence of ΔU and ΔS.

Conflicts of interest

There are no conflicts to declare.

Acknowledgments

References

(1) Toal, S.; Schweitzer-Stenner, R. Local order in the unfolded state: conformational biases and nearest neighbor interactions. *Biomolecules* **2014**, *4*, 725–773.

(2) Liu, Z.; Chen, K.; Ng, A.; Shi, Z.; Woody, R. W.; Kallenbach, N. R. Solvent dependence of P_{II} conformation in model alanine peptides. *J. Am. Chem. Soc.* **2004**, *126*, 15141–15150.

(3) Kang, Y. K. Conformational preferences of non-prolyl and prolyl residues. *J. Phys. Chem. B* **2006**, *110*, 21338–21348.

(4) Toal, S.; Amidi, O.; Schweitzer-Stenner, R. Conformational changes of trialanine induced by direct interactions between alanine residues and alcohols in binary mixtures of water with glycerol and ethanol. *J. Am. Chem. Soc.* **2011**, *133*, 12728–12739.

(5) Milorey, B.; Farrell, S.; Toal, S. E.; Schweitzer-Stenner, R. Demixing of water and ethanol causes conformational redistribution and gelation of the cationic GAG tripeptide. *Chem. Commun.* **2015**, *51*, 16498–16501.

(6) Sreerama, N.; Woody, R. W. Poly (Pro) II helixes in globular proteins: Identification and circular dichroic analysis. *Biochemistry* **1994**, *33*, 10022–10025.

(7) Poon, C.-D.; Samulski, E. T.; Weise, C. F.; Weisshaar, J. C. Do bridging water molecules dictate the structure of a model dipeptide in aqueous solution? *J. Am. Chem. Soc.* **2000**, *122*, 5642–5643.

(8) Schweitzer-Stenner, R.; Eker, F.; Huang, Q.; Griebenow, K. Dihedral angles of trialanine in D_2O determined by combining FTIR and polarized visible Raman spectroscopy. *J. Am. Chem. Soc.* **2001**, *123*, 9628–9633.

(9) Woutersen, S.; Mu, Y.; Stock, G.; Hamm, P. Subpicosecond conformational dynamics of small peptides probed by two-dimensional vibrational spectroscopy. *Proc. Natl. Acad. Sci. U.S.A.* **2001**, *98*, 11254–11258.

(10) Shi, Z.; Olson, C. A.; Rose, G. D.; Baldwin, R. L.; Kallenbach, N. R. Polyproline II structure in a sequence of seven alanine residues. *Proc. Natl. Acad. Sci. U.S.A.* **2002**, *99*, 9190–9195.

(11) Schweitzer-Stenner, R.; Measey, T. J. The alanine-rich XAO peptide adopts a heterogeneous population, including turn-like and polyproline II conformations. *Proc. Natl. Acad. Sci. U.S.A.* **2007**, *104*, 6649–6654.

(12) Takekiyo, T.; Imai, T.; Kato, M.; Taniguchi, Y. Temperature and pressure effects on conformational equilibria of alanine dipeptide in aqueous solution. *Biopolymers* **2004**, *73*, 283–290.

(13) Smith, P. E. The alanine dipeptide free energy surface in solution. *J. Chem. Phys.* **1999**, *111*, 5568–5579.

(14) Vymetal, J.; Vondrasek, J. Metadynamics as a tool for mapping the conformational and free-energy space of peptides the alanine dipeptide case study. *J. Phys. Chem. B* **2010**, *114*, 5632–5642.

(15) Pettitt, B. M.; Karplus, M. The potential of mean force surface for the alanine dipeptide in aqueous solution: A theoretical approach. *Chem. Phys. Lett* **1985**, *121*, 194–201.

(16) Tobias, D. J.; Brooks III, C. L. Conformational equilibrium in the alanine dipeptide in the gas phase and aqueous solution: A comparison of theoretical results. *J. Phys. Chem.* **1992**, *96*, 3864–3870.

(17) Okumura, H.; Okamoto, Y. Temperature and pressure dependence of alanine dipeptide studied by multibaric- multithermal molecular dynamics simulations. *J. Phys. Chem. B* **2008**, *112*, 12038–12049.

(18) Barducci, A.; Bussi, G.; Parrinello, M. Well-tempered metadynamics: A smoothly converging and tunable free-energy method. *Phys. Rev. Lett.* **2008**, *100*, 020603.

(19) Bonomi, M.; Barducci, A.; Parrinello, M. Reconstructing the equilibrium Boltzmann distribution from well-tempered metadynamics. *J. Comp. Chem.* **2009**, *30*, 1615–1621.

(20) Dama, J. F.; Rotskoff, G.; Parrinello, M.; Voth, G. A. Transition-tempered metadynamics: Robust, convergent metadynamics via on-the-fly transition barrier estimation. *J. Chem. Theor. Comp.* **2014**, *10*, 3626–3633.

(21) Apostolakis, J.; Ferrara, P.; Caflisch, A. Calculation of conformational transitions and barriers in solvated systems: Application to the alanine dipeptide in water. *J. Chem. Phys.* **1999**, *110*, 2099–2108.

(22) Pettitt, B. M.; Karplus, M. Conformational free energy of hydration for the alanine dipeptide: Thermodynamic analysis. *J. Phys. Chem.* **1988**, *92*, 3994–3997.

(23) Marsili, S.; Barducci, A.; Chelli, R.; Procacci, P.; Schettino, V. Self-healing umbrella sampling: A non-equilibrium approach for quantitative free energy calculations. *J. Phys. Chem. B* **2006**, *110*, 14011–14013.

(24) Drozdov, A. N.; Grossfield, A.; Pappu, R. V. Role of solvent in determining conformational preferences of alanine dipeptide in water. *J. Am. Chem. Soc.* **2004**, *126*, 2574–2581.

(25) Cuny, J.; Korchagina, K.; Menakbi, C.; Mineva, T. Metadynamics combined with auxiliary density functional and density functional tight-binding methods: Alanine dipeptide as a case study. *J. Mol. Model* **2017**, *23*, 72.

(26) Wang, Z.-X.; Duan, Y. Solvation effects on alanine dipeptide: A MP2/cc-pVTZ//MP2/6-31G** study of (Φ, Ψ) energy maps and conformers in the gas phase, ether, and water. *J. Comput. Chem* **2004**, *25*, 1699–1716.

(27) Gimondi, I.; Tribello, G. A.; Salvalaglio, M. Building maps in collective variable space. *J. Chem. Phys.* **2018**, *149*, 104104.

(28) Iwasaki, H.; Yamaguchi, S.; Miura, S. Comparative study of 3D-RISM theory and molecular dynamics calculations for the free-energy landscape of a hydrated dipeptide. *Mol. Simul.* **2017**, *43*, 1406–1411.

(29) Piskulich, Z. A.; Thompson, W. H. On the temperature dependence of liquid structure. *J. Chem. Phys.* **2020**, *152*, 011102.

(30) Piskulich, Z. A.; Thompson, W. H. Temperature dependence of the water infrared spectrum: Driving forces, isosbestic points, and predictions. *J. Phys. Chem. Lett.* **2020**, *11*, 7762–7768.

(31) Mahynski, N. A.; Errington, J. R.; Shen, V. K. Temperature extrapolation of multicomponent grand canonical free energy landscapes. *J. Chem. Phys.* **2017**, *147*, 054105.

(32) Mahynski, N. A.; Errington, J. R.; Shen, V. K. Multivariable extrapolation of grand canonical free energy landscapes. *J. Chem. Phys.* **2017**, *147*, 234111.

(33) Mahynski, N. A.; Jiao, S.; Hatch, H. W.; Blanco, M. A.; Shen, V. K. Predicting structural properties of fluids by thermodynamic extrapolation. *J. Chem. Phys.* **2018**, *148*, 194105.

(34) Sugita, Y.; Okamoto, Y. Replica-exchange molecular dynamics method for protein folding. *Chem. Phys. Lett.* **1999**, *314*, 141–151.

(35) Wang, J.; Cieplak, P.; Kollman, P. A. How well does a restrained electrostatic potential (RESP) model perform in calculating conformational energies of organic and biological molecules? *J. Comp. Chem.* **2000**, *21*, 1049–1074.

(36) Jorgensen, W. L.; Chandrasekhar, J. M.; JD, I. RW; Klein, MLJ Chem. *Phys* **1983**, *79*, 926.

(37) Lindahl, E.; Hess, B.; Van Der Spoel, D. GROMACS 3.0: A package for molecular simulation and trajectory analysis. *Molecular modeling annual* **2001**, *7*, 306–317.

(38) Tribello, G. A.; Bonomi, M.; Branduardi, D.; Camilloni, C.; Bussi, G. PLUMED 2: New feathers for an old bird. *Comp. Phys. Commun.* **2014**, *185*, 604–613.

(39) Nosé, S. A molecular dynamics method for simulations in the canonical ensemble. *Mol. Phys.* **1984**, *52*, 255–268.

(40) Hoover, W. G. Canonical dynamics: Equilibrium phase-space distributions. *Phys. Rev. A* **1985**, *31*, 1695–1697.

(41) Essmann, U.; Perera, L.; Berkowitz, M. L.; Darden, T.; Lee, H.; Pedersen, L. G. A smooth particle mesh Ewald method. *J. Chem. Phys.* **1995**, *103*, 8577–8593.

(42) Shoemaker, D. P.; Garland, C. W.; Nibler, J. W. *Experiments in Physical Chemistry*; McGraw-Hill: New York, 1989.

(43) Madison, V.; Kopple, K. D. Solvent-dependent conformational distributions of some dipeptides. *J. Am. Chem. Soc.* **1980**, *102*, 4855–4863.

(44) Parchansky, V.; Kapitan, J.; Kaminsky, J.; Sebestík, J.; Bour, P. Ramachandran plot for alanine dipeptide as determined from Raman optical activity. *J. Phys. Chem. Lett.* **2013**, *4*, 2763–2768.

(45) Graf, J.; Nguyen, P. H.; Stock, G.; Schwalbe, H. Structure and dynamics of the homologous series of alanine peptides: A joint molecular dynamics/NMR study. *J. Am. Chem. Soc.* **2007**, *129*, 1179–1189.

(46) Kim, Y. S.; Wang, J.; Hochstrasser, R. M. Two-dimensional infrared spectroscopy of the alanine dipeptide in aqueous solution. *J. Phys. Chem. B* **2005**, *109*, 7511–7521.

TOC Graphic